

# The Variable Optical Polarization and *FERMI* Observations of PMN J0948+0022

Joseph R. Eggen, H. Richard Miller, Jeremy D. Maune

Department of Physics and Astronomy, Georgia State University, Atlanta, GA 30303-3083

eggen@chara.gsu.edu

Received \_\_\_\_\_;    accepted \_\_\_\_\_

## Abstract

We report on observations of the  $\gamma$ -ray and optical photopolarimetric behavior of the radio-loud, narrow line type-1 Seyfert galaxy PMN J0948+0022 over a twenty seven month period. As this object has recently been suggested to represent a prototype of an emerging class of blazar-like objects, the observed properties are compared to those of blazars. We extract doubling timescales of roughly 4 hours for the optical and  $\gamma$ -ray bands. The rapid microvariability in the optical/NIR, significant and variable optical polarization, and strong yet rapidly-variable  $\gamma$ -ray emission we observe for PMN J0948+0022 are all classical observational characteristics associated with blazars. However, since these observations do not show a clear correlation between the  $\gamma$ -ray and optical behavior, they do not offer conclusive proof that the emissive behavior of PMN J0948+0022 is due to a relativistic jet oriented close to our line of sight.

*Subject headings:* galaxies: active – galaxies: individual: J0948+0022 – galaxies: photometry – galaxies: polarimetry – galaxies: Seyfert

## 1. Introduction

Recently, several members of a sub-class of active galactic nuclei have been observed with properties that would have previously been divided among Seyfert galaxies, Broad Line Radio Galaxies (BLRG), and blazars. These objects, the Radio-Loud Narrow Line Type-1 Seyferts (RL NLS1), possess the standard identifying properties of NLS1 (Osterbrock & Pogge 1985; Kellermann et al. 1989): strong optical emission of FeII, weak emission from forbidden lines (i.e.  $[\text{OIII}]/\text{H}\beta < 3$ ), and  $\text{FWHM}(\text{H}\beta) \leq 2000 \text{ km/s}$  (Goodrich, R. W. 1989). However, the property of radio-loudness ( $R \geq 10$ , where  $R = f_{5.0 \text{ GHz}}/f_{4400\text{\AA}}$ ) (Kellermann et al. 1989) is markedly rare in galaxies of this type, occurring in  $< 7\%$  of such systems (Komossa et al. 2006). High brightness temperature ( $\geq 10^{13}\text{K}$ ), radio (Zhou et al. 2003) loudness, and strong/rapid variability are, however, properties of blazars. It is the combination of these various observational properties that lead many to now believe that RL NLS1 and blazars may both play host to relativistic jets.

It is now widely accepted that all varieties of Active Galactic Nuclei (AGN) are manifestations of the same basic phenomenon - accretion of matter onto a Supermassive Black Hole (SMBH) at the center of a galaxy. The different classes of AGN that we then observe result, to a large degree, from these objects being oriented differently with respect to our line of sight. Blazars, a class of AGN characterized by strong and variable emission across all wavelengths and strong and highly variable polarization in the radio and optical (Blandford & Rees 1978), are believed to result from the orientation of our line-of-sight near the axis of a relativistic jet of particles being emitted from the central engine of the source. Until recently, blazars were almost exclusively observed to be hosted in elliptical galaxies, with very few exceptions (McHardy et al 1994). Since the majority of NLS1 hosts are spiral galaxies, finding evidence of blazar-like behavior in such systems would help to fill in a curiously barren demographic of the blazar population.

PMN J0948+0022 is an object that displays the expected properties of a Narrow-Line Seyfert-1 galaxy as described above (Zhou et al. 2003), as well as those of blazars, such as strong and variable emission in the radio thru  $\gamma$ -ray energies over long timescales (Abdo et al. 2009; Foschini et al. 2012), and microvariability in the optical (Maune et al. 2013). Ikejiri et al. (2011) also observed PMN J0948+0022 to exhibit a very high degree of linear polarization (18.8%) in the optical (V-band), when the object was very bright ( $V = 17.028 \pm 0.014$ ).

To date, no comprehensive, long-term program investigating the optical polarimetric/photometric characteristics of RL NLS1 has been reported. This paper provides the results of such a study for the prototype for this class of objects, PMN J0948+0022.

Throughout this manuscript, Julian Dates (JD) are expressed as Modified Julian Dates MJD. The conversion to MJD is expressed as  $MJD = JD - 2.45e6$ .

## 2. Observations and Data Reductions

### 2.1. Optical Photopolarimetry Data

All optical polarimetric data used in this study were obtained with the 72-inch Perkins telescope at Lowell Observatory in Flagstaff, Arizona, using the PRISM instrument which includes a polarimeter with a rotating half-wave plate. Data were obtained during several observing runs between February, 2011 and April, 2013. The specific dates of each observation are given in Table 1. The observations consisted of a series of 2-4 measurements for the Q and U Stokes parameters per polarization observation. Each series consisted of four images, each taken at different instrumental position angles –  $0^\circ$ ,  $45^\circ$ ,  $90^\circ$ , and  $135^\circ$  – of the waveplate.

Corrections to polarimetric values were obtained from two sources: in-field comparison

stars and separately-observed polarimetric standards, both polarized and unpolarized (Schmidt et al. 1992). As the camera has a wide field of view (approx.  $14' \times 14'$ ), we are able to use field stars for interstellar polarization corrections by subtracting the average percent polarization of the brightest field stars. Polarized and unpolarized standard stars are used to calibrate corrections for polarization Position Angle (P.A.) and instrumental polarization (typically less than 1%) (Jorstad et al. 2010), respectively.

The data were reduced and analyzed using in-house scripts, which utilize standard packages in the PyRAF 2.0 suite of reduction tools<sup>1</sup>. Bias frames were taken at the beginning of every night and combined into a master bias that was subtracted from each image. Flat frames were taken at least once per run, using a featureless screen inside the dome. Each position of the waveplate required its own set of flats, which would later be combined into one master flat per position angle for application to the appropriate science image(s). Cosmic ray cleaning was performed on all science images, with the **threshold** and **fluxratio** parameters set to 35 and 5, respectively. Aperture photometry was then performed on the calibrated science frames on an object-by-object basis. An aperture radius of 7 arcsec was used on all images both to maximize the signal-to-noise and to maintain consistency with the optical photometry being performed on this target by Maune et al. (2013). Use of the in-field comparison stars compiled by Maune et al. allowed for one to obtain simultaneous measures of the absolute R-band magnitude, as well as the percent polarization (P) and electric vector position angle (EVPA).

For ease-of-comparison with  $\gamma$ -ray data, which are expressed as photon fluxes in this manuscript, optical data were converted from magnitudes to units of flux (mJy) using the following equation:

---

<sup>1</sup>PyRAF is a product of the Space Telescope Science Institute, which is operated by AURA for NASA.

$$F = 2941 * 10^{-0.4*Mag} \quad (1)$$

Where  $F$  is the flux in mJy and  $Mag$  is the R-band magnitude.

## 2.2. Optical and Infrared Photometry with SMARTS

Much of our optical and all of our NIR data were obtained by the 1.3m telescope at the Cerro Tololo Inter-American Observatory (CTIO) under the Small and Moderate Aperture Research Telescope System (SMARTS) program. We obtained simultaneous data in the optical R and infrared J bands using ANDICAM, which is a dual-channel instrument that uses a dichroic to simultaneously feed optical and IR CCD imagers, allowing the acquisition of IR data from 0.4 to 2.2  $\mu\text{m}$ . Our limited dataset of J-band images consisted of four NIR images - one for each corresponding optical R-band image - which were flat-fielded, overscan-corrected, bias-subtracted, and co-added using standard PyRAF/IRAF packages and scripts. To be consistent with our optical data, a 7 arcsec aperture radius was used to perform differential photometry.

## 2.3. *FERMI*-LAT Data

Gamma-ray data were obtained through the *FERMI*-LAT public data server. The Large Area Telescope (LAT), on board the *FERMI* Gamma-ray Space Telescope, is a pair-conversion detector sensitive to  $\gamma$ -rays in the 20 MeV to several hundred GeV energy range (Atwood et al. 2009). The instrument has worked almost continuously in all-sky-survey mode since its launch in June 2008, which allows coverage of the entire  $\gamma$ -ray sky approximately every 3 hours. The data were reduced and analyzed using ScienceTools v9r27p1 and instrument response functions P7SOURCE\_V6. We utilized the likelihood

analysis procedure as described at the FSSC website. Photon fluxes were calculated using data from MJD 5562 to MJD 6408 (January 01, 2011 to April 25, 2013).

Our data were downloaded from the FERMI website on March 27, 2013 and cover a region on the sky  $15^\circ$  in radius, centered on the location of PMN J0948+0022 (2FGL0948.8+0020 from the Fermi 2-Year Point Source Catalog), and in an energy range of 100 MeV to 300 GeV. Our  $\gamma$ -ray light curve consists of 112 equally-sized bins, each of which is 637861 seconds in length, or one-quarter of the lunar synodic period, as our observing runs at Lowell Observatory were centered around the time of the New Moon. The first bin began on February 03, 2011, while the last bin ended on April 25, 2013. Only data corresponding to the SOURCE class (evclass=2) were utilized, with a  $52^\circ$  cut-off rock-angle of the spacecraft, while an additional cut utilizing an angle of  $100^\circ$  from the zenith was imposed so as to minimize the contamination due to  $\gamma$ -rays coming from Earth’s upper atmosphere. Since PMN J0948+0022 is within  $20^\circ$  of the ecliptic, and the Sun is a source of  $\gamma$ -rays comparable to our target (Abdo et al. 2011b), a final cut was used to exclude exposures that occurred when the Sun was within the  $10^\circ$  Region of Interest (RoI). Photon fluxes and spectral fits were derived using an unbinned maximum likelihood analysis which was accomplished using the ScienceTool GTLIKE.

In order to accurately measure the flux and spectral parameters of the source, one needs to account for  $\gamma$ -rays emitted from the background. To this end, two models were used: an isotropic background model accounting for extragalactic diffuse emission and residual charged particle background, and a Galactic diffuse emission model to account for diffuse sources from within our own galaxy. The isotropic model we used was the one contained in the file iso\_p7v6source.txt<sup>2</sup>, while the Galactic component was given by the file gal\_2year7v6\_v0.fits. The normalizations of both components were left to vary freely

---

<sup>2</sup><http://fermi.gsfc.nasa.gov/ssc/data/access/lat/Background/Models.html>

during likelihood analysis.

In order to determine the significance of the  $\gamma$ -ray signal from PMN J0948+0022, we used the Test Statistic (TS). The Test Statistic is defined as  $TS = 2\Delta\log(\text{likelihood})$ , where *likelihood* refers to the likelihood ratio test as described in Mattox et al. (1996). Determining the likelihood of a given photon flux being produced by a source with a given spectral model was accomplished using the GTLIKE Science Tool. Our source model consisted of all the known  $\gamma$ -ray point sources located within a  $15^\circ$  radius of 2FGLJ0948.8+0020. Initial values for all spectral parameters for these sources were taken from the LAT 2-year Point Source Catalog. Along with PMN J0948+0022 and the aforementioned background models, several point sources were allowed to vary (i.e. photon indices, normalization factors, and spectral slope indices were left as free parameters) during the likelihood analysis, so as to account for the inherent variability of many  $\gamma$ -ray sources. The type of spectral model used for a given source was the same model used for that source in the LAT 2-year catalog (Nolan et al. 2012).

For PMN J0948+0022 specifically, we used a LogParabola model to describe the  $\gamma$ -ray spectrum of the source in this study. This model takes the form:

$$N(E) = N_0 \left( \frac{E}{E_b} \right)^{\alpha + \beta \ln(E/E_b)} \quad (2)$$

where  $N_0$  is the normalization index,  $\alpha$  is the photon index at the pivot energy  $E_b$ , and  $\beta$  is the curvature index. These parameters were left un-fixed with the exception of  $E_b$ : this was fixed at a value of 271.597 MeV, which is the value reported for this object in the LAT 2-year catalog. All  $\gamma$ -ray fluxes presented in this paper are integrated over the entire energy range cited above (100 MeV to 300 GeV), with corresponding units of  $[\text{ph cm}^{-2}\text{sec}^{-1}]$ .

Sources outside our  $10^\circ$  Radius of Interest (RoI) but within  $20^\circ$  of the target were also included in the source model, as the point spread functions of these objects could result



in extra photons seeping into the RoI of our target. All parameters for these sources were fixed to their 2FGL catalog values during the analysis.

### 3. Results

#### 3.1. Polarimetry

Our polarimetric results are detailed in Table 1 and displayed for comparison in Fig. 1. The top panel of Figure 1 also displays the all of our optical data for comparison, binned in 24-hour increments as described in Section 3.2, below. Note that all photometric data points in the aforementioned table and 2nd panel of Figure 1 were derived from polarimetric measurements. PMN J0948+0022 displays a moderate, but significant variability in both the percent polarization (P) and EVPA, with a maximum P of  $12.31 \pm 1.21\%$  and an EVPA which varied substantially. While there does seem to be evidence for a correlation between the optical state and the polarimetric quantities in the data - a high optical state coupled with a high value of P, for example - the data also contains notable exceptions to such a relationship (e.g., the lack of any increase in P during an outburst in early 2013). No significant correlation was observed between the optical or polarimetric quantities and the  $\gamma$ -ray flux. It should also be noted that the  $180^\circ$  uncertainty inherent in the measurement of the position angle may produce the appearance of trends where none exist.

A plot of each value of P versus the concurrent R-magnitude is shown in Figure 2. A clear trend between these two values is not immediately obvious. However, closer inspection of the three brightest data points revealed notable characteristics. The brightest data point (corresponding to the data from MJD = 5706.7 in Table 1) also represents the largest value of P and was taken when the object was observed to be in a persistent (42-minute duration) and stable (variation of  $0.35 \pm .05$  magnitudes) bright state. The second-highest point

corresponds to the data at  $\text{MJD} = 6300.0$  from Table 1 and occurred 4.44 hours after the object was observed to be  $0.75 \pm .02$  magnitudes fainter via differential photometry. The third-brightest point was obtained 24 hours before the brightest data point and though they differ in time and brightness by relatively very little, they have quite different polarimetric values. Possible interpretations of these observations are discussed later in Section 4.

### 3.2. R-band Photometry

The optical photometric data utilized in the present study were obtained from the following sources: (1) polarimetry obtained by the group at Georgia State University (Table 1), (2) optical data presented in Maune et al. (2013), and (3) additional data collected since the publication of Maune et al.. These datasets were merged to make a master optical light curve, which contained 1321 R-band observations obtained between February 7, 2011, and April 19, 2013. A program was written which binned the optical data with the same temporal bounds as the  $\gamma$ -ray data. An average value was then calculated for each bin to provide a single data point (42 optical photometric data points in total, displayed in Figure 3), allowing us to better-match the optical photometric data to the cadence of the *FERMI* observations. We also binned the R-band data in 24-hour bins centered on 00:00 UT, as the latitudes at which our data were obtained resulted in acquisition times roughly centered on this time of day. The 24-hour binned data (114 data points) can be seen in the top panel of Figure 1 and are also accessible via the online version of this manuscript. A sample of this data is provided in Table 2. This technique also served to “smooth” some of the large changes in the optical flux over short time periods that are often manifest in PMN J0948+0022 (see below).

By making use of high-cadence data presented in our previous work, as well as new data obtained in January of 2013, we were able to make very precise measurements of the

doubling/halving timescale ( $\tau$ ) for this object in the R-band. The formula for calculating the observed timescale  $\tau$  is given by the equation (Foschini et al. 2011):

$$F(t) = F(t_0) * 2^{-(t-t_0)/\tau} \quad (3)$$

where  $F(t)$  and  $F(t_0)$  are flux values at the times  $t$  and  $t_0$ , respectively. Throughout the remainder of this manuscript we will use  $\tau_R$  and  $\tau_\gamma$  to refer to the doubling timescales measured for the optical R and  $\gamma$ -ray bands, respectively.

This quantity was calculated for PMN J0948+0022 in several wavebands by Foschini et al. (2012), although they did not have access to significant micro-variability data (especially in the optical bands) in their study. Micro-variability data collected by the present authors on two nights were used to calculate  $\tau_R$ , and are shown in Figures 4 and 5. Figure 4 (first presented in Maune et al. (2013)) reveals the target to be highly variable on very short (a few minutes) timescales, with the object going from a minimum brightness of  $R = 18.69 \pm .02$  to a maximum of  $R = 17.92 \pm .02$  in 4.45 hours. This resulted in a doubling timescale of  $\tau_R = 4.39 \pm .19$  hours. Conversely, Figure 5 (original to this work) illustrates a rapid decrease in the brightness of PMN J0948+0022, though over a similar magnitude range and duration as the doubling event. Here we see the object fall from  $R = 18.13 \pm .04$  to  $R = 18.96 \pm .02$  in 3.97 hours, for a halving timescale of  $\tau_R = 3.60 \pm .23$  hours. Together, these lightcurves yield an average value of  $\tau_R = 3.99 \pm .15$  hours.

Concerning the aforementioned Figures, there are two items of note. The first is that the above value for  $\tau_R$  should be taken as an upper limit. The gaps in the lightcurves presented in Figures 4 and 5 may contain higher or lower flux states which would drastically reduce the doubling timescale. The second item is that both lightcurves show discrete brightening events (flares - three in total) that are not only well-sampled, but also roughly symmetric in their brightening and dimming profiles and are on the order of an hour in

duration.

In March 2013, PMN J0948+0022 underwent a dramatic brightening in the R-band (Figure 6), achieving a maximum brightness of  $R = 17.140 \pm 0.021$ , which was unprecedented for the object in this band. We were fortunate to have obtained simultaneous J-band data during this flaring episode, although we currently lack calibrated values for field stars in the J-band. However, as can be seen in Table 3, the degree of the fractional change of the optical flux was closely mirrored by that in the NIR flux. Interestingly, there was no indication of correlated activity in the  $\gamma$ -ray regime, on any timescale, which could be linked to the optical/NIR activity. While correlation of activity across multiple wavebands is a common characteristic of blazars (see, for example, Rani et al. (2013), Abdo et al. (2010)), it is also not unusual to find examples of high activity in one band without the presence of similar activity in other bands (Krawczynski et al. 2004).

### 3.3. $\gamma$ -ray Observations

The long-term behavior of PMN J0948+0022 in  $\gamma$ -rays is shown in Fig. 3. Our long-term  $\gamma$ -ray dataset consists of 112 data points in total, including 31 upper limit values. The TS value may be used as a proxy for the confidence in the measurement, with  $TS \geq 9$  (corresponding roughly to  $\sigma \geq 3$ ) (Mattox et al. 1996) being the threshold above which we considered a positive detection. We applied the method for extracting upper limits, as described on the *FERMI* website<sup>3</sup>, to bins with  $TS < 9$ . As PMN J0948+0022 is a well-established  $\gamma$ -ray source (Abdo et al. 2009), and less than 1/3 of our data points are below this threshold, we feel it is reasonable to treat all of our remaining gamma-ray data points as direct detections.

---

<sup>3</sup>[http://fermi.gsfc.nasa.gov/ssc/data/analysis/scitools/python\\_tutorial.html](http://fermi.gsfc.nasa.gov/ssc/data/analysis/scitools/python_tutorial.html)

PMN J0948+0022 was observed to undergo a significant increase in  $\gamma$ -ray brightness in the spring of 2011, which was mirrored by a steady increase of the average R-band luminosity over the next few months, as can be seen in the top 2 panels of Fig. 3. Unfortunately, the  $\gamma$ -ray brightening which was observed in the spring of 2001 continued into the summer when PMN J0948+0022 could not be viewed in the optical due to the close proximity of the Sun. Nevertheless, when optical monitoring resumed in November 2011, the object was observed to be back at a low state in both the optical and  $\gamma$ -rays and would remain in that state until the end of optical monitoring in the spring of 2012. The resumption of optical monitoring in the fall of 2012 was accompanied by an increase in  $\gamma$ -ray activity which was dominated by two especially active periods centered roughly on MJD 6225 and 6290. Perhaps most interestingly, the optical activity remained generally much higher than average after MJD 6300, even though  $\gamma$ -ray activity dropped to a relatively inactive state.

On December 18, 2012, PMN J0948+0022 was observed to undergo a flare in the near-infrared (Carrasco et al. 2012), followed by a strong  $\gamma$ -ray peak as observed by FERMI-LAT (D’Ammando & Orienti 2013). The measured flux for the bin in which the peak of this event fell (MJD = 6294) was  $9.22 \times 10^{-7}$  ph cm $^{-2}$ s $^{-1}$ , with a TS = 194.27. Due to the strength of this event, we were able to bin the data to much higher cadence (6 hours) around the peak of the flare. Figure 7 illustrates the rapidly-evolving nature of the flare with 24-hour (top panel) and 6-hour (bottom panel) bins. One quickly notices that the flux appears to double twice (within a 2- $\sigma$  uncertainty) in the 6-hour light curve. Applying Eq. 3.2 to the relevant bins yields a measurement of the doubling timescale in the  $\gamma$ -ray regime of  $\tau_{\gamma} = 3.55 \pm 4.29$  hours - see Table 4 for the values used to calculate this result. A doubling timescale of approximately 4 hours not only roughly agrees with our measurement of  $\tau_R$ , but is also comparable to the  $\gamma$ -ray variability timescales found for 3C 454.3 during that object’s recent outbursts in 2009 (Ackermann et al. 2010) and 2010

(Abdo et al. 2011a), who found doubling timescales of 3 hours and 6 hours, respectively.

#### 4. Discussion & Conclusions

Multi-epoch VLBA observations of a number of  $\gamma$ -ray detected quasars and blazars (Jorstad et al. 2001) suggest that the  $\gamma$ -ray emission observed for these objects originates near the radio core, perhaps corresponding to a standing shock in the jet itself, and not specifically originating from a location near the central SMBH. It is thought that the oft-observed flares are produced as a result of turbulence/instabilities, which are present in the relativistic jet and arise as shocks in this outflow. With the passage of a shock down the jet, the magnetic field will be compressed within the shock region causing the field to become more highly ordered. Observationally, one would then expect that the fractional linear polarization would increase and the direction of the electric vector position angle would change rapidly.

The present observations allow us to evaluate if this is the case for the  $\gamma$ -ray/optical flux variations observed for PMN J0948+0022. In Fig. 3 we have plotted the  $\gamma$ -ray and optical light curves for 2011-2013. A possible correlation between the optical and  $\gamma$ -ray regimes is suggested in parts of the dual lightcurve. To further evaluate this, in Figure 8 we have plotted the optical flux versus the  $\gamma$ -ray flux. While we do not see any evidence of a strong correlation, we do note that above a certain threshold in the  $\gamma$ -ray brightness (approximately  $2 \times 10^{-7}$  ph cm $^{-2}$  s $^{-1}$ ), we consistently see the object in an elevated optical state (approximately  $9.5 \times 10^{-5}$  mJy or  $R \leq 18.7$ ). However, the converse is not true: we do not always see PMN J0948+0022 in an elevated  $\gamma$ -ray state when it is optically bright - even during periods of extended and dramatic brightening, such as that of the period in March 2013 as detailed in Figure 6. The absence of a strong correlation suggests that there is substantial turbulence present in the jet and the magnetic field is not highly ordered, in

turn suggesting that no strong shock is present during the time of these observations.

The picture becomes more complicated if we look at the photopolarimetry data as displayed in Figure 2. This plot appears to show a potential bi-modal distribution in the P vs. R-mag plane. A positive correlation between these values could be seen as supporting the so-called shock-in-jet interpretation (Marscher et al. 2008), though several data points, especially in the high-magnitude, low-polarization part of the figure, strongly disagree with this interpretation. However, as was noted in section 3.1, the two brightest, low-polarization points occurred during times of rapid flux variation in the object, which may indicate that these “errant” data were the result of turbulence in part of the jet, rather than a standing shock affecting the entire optical emitting region.

Our measurements for the doubling timescales in the R-band and  $\gamma$ -rays -  $\tau_R$  and  $\tau_\gamma$ , respectively - provide additional insight into the variability nature of PMN J0948+0022. As stated in Sections 3.2 & 3.3, the doubling timescale in the optical ( $\tau_R$ ) was  $3.99 \pm .15$  hours while the corresponding quantity in the  $\gamma$ -ray regime ( $\tau_\gamma$ ) was  $3.55 \pm 4.29$  hours. These values represent a significantly faster doubling timescale for this object as compared to those presented by Foschini et al. (2012), who found the values of  $\tau$  in the optical or  $\gamma$ -ray bands to be on the order of 2-4 days. The close agreement of the values presented in this work for  $\tau_R$  and  $\tau_\gamma$  could be used to argue in favor of comparable sizes for the emitting regions of both the optical and high-energy radiation, implying that these regions are located close to each other along the jet, though not necessarily co-spatial. Localized turbulence in part of the jet, rather than (or in addition to) some sort of standing shock, may better explain the observed behavior.

It is, perhaps, not surprising that the short variability timescales of this object have gone undetected in previous studies, as it required several dedicated optical observing runs and constant monitoring at high energies to obtain data of sufficient quality to deduce

such values for this work. Over two dozen nights of high-cadence, focused observations in the optical were required to obtain the two nights of data that allowed us to calculate  $\tau_R$ , whilst an exceptional episode of  $\gamma$ -ray emission in terms of both flux and confidence in the measurement was required to determine  $\tau_\gamma$ . Clearly, the observed behavior of PMN J0948+0022 is very complex and may require the application of models that take into account turbulence as well as shocks in the jet to explain this behavior adequately. All of this underscores the important role that dedicated, long-term monitoring programs can play in studying objects of this type.

## 5. Summary

In this work we have identified many common properties of blazars which seem to be present in PMN J0948+0022. These include a strong linear polarization which is highly variable in both the percentage of polarization (P) and orientation of the electric vector (EVPA), an optical flux which varied by more than 2.88 magnitudes over the twenty seven month observation period, infrared/optical flaring which was observed to have no  $\gamma$ -ray counterpart, and upper limits for the doubling timescales in both the optical and  $\gamma$ -ray regimes which were both measured to be very fast (around 4 hours).

We have also observed what may be evidence for localized turbulence in the jet, in the form of strong brightening events with no corresponding increase in the value of P, extremely rapid doubling timescales in the optical and  $\gamma$ -ray regimes, and strong/rapid flares in the optical & infrared which have no  $\gamma$ -ray counterpart.

While the present observations do not allow one to definitively confront the model suggesting that the  $\gamma$ -ray emission is produced at a shock, down-stream in the jet, some distance from the SMBH, it does suggest what is required: It will require quasi-



simultaneous  $\gamma$ -ray and optical/photopolarimetric observations during a major  $\gamma$ -ray/optical flare consisting of a change in flux significantly greater than a factor of three, such as was observed in the present campaign. Under these conditions, one should be able to determine if there is a significant increase in the polarization (P) and the expected rapid change in the electric vector position angle (EVPA) accompanying such an outburst. Therefore we encourage continued photopolarimetric monitoring of this object in order to investigate the behavior of the polarization during the next major outburst of PMN J0948+0022.

The authors would like to thank Svetlana Jorstad and Paul Smith for their comments, assistance, and technical expertise.

## REFERENCES

- Abdo, A. A., et al., 2009, ApJ, 707, 727
- Abdo, A. A., et al., 2010, Nature, 463, 919
- Abdo, A. A., et al., 2011a, ApJ, 733, L26
- Abdo, A. A., et al. 2011b, ApJ, 734, 116
- Ackermann, M., et al., 2010, ApJ, 721, 1383
- Atwood W. B., et al., 2009, ApJ, 697, 1071
- Blandford, R., Rees, M., 1978, in Wolfe A. N., ed., Pittsburgh Conference on BL Lac Objects. Pittsburgh Univ. Press, Pittsburgh, PA, p. 328
- Carrasco, L., et al., 2012, Astron. Telegram, 4659
- D’Ammando, F., Orienti, M., 2013, Astron. Telegram, 4694
- Foschini, L., Ghisellini, G., Tavecchio, F., Bonnoli, G., Stamerra, A. 2011, A&A, 530, A77
- Foschini, L., et al., 2012, A&A, 548, A106
- Goodrich, R. W., 1989, ApJ, 342, 224
- Ikejiri, Y., et al., 2011, Publ. Astron. Soc. Japan, 63, 639
- Jorstad, S. G., et al., 2001, ApJ, 556, 738
- Jorstad, S. G., et al., 2010, ApJ, 715, 362
- Kellermann, K., Sramek, R., Schmidt, M., Shaffer, D. B., Green, R. 1989, AJ, 98, 1195
- Komossa, S., Voges, W., Xu, D., Mather, S., Adorf, H., Lemson, G., Duschl, W. J., Grupe D. 2006, AJ, 132, 531

Krawczynski, H. et al., 2004, ApJ, 601, 151

Mattox, J. R., et al., 2006, ApJ, 461, 396

Marscher et al., 2008, Nature, 452, 966

Maune, J. D., Miller, H. R., Eggen, J. R. 2013, ApJ, 762, 124

McHardy, I. M., Merrifield, M. R., Abraham, R. G., Crawford, C. S., 1994, MNRAS, 268,  
681

Nolan, P. L., et al., 2012, ApJS, 199, 31

Osterbrock, D. E., Pogge, R. W., 1985, ApJ, 297, 166

Rani, B., et al., 2013, A&A, 552, A11

Schmidt, G. D., Elston, R., Lupie, O. L., 1992, AJ, 104, 1563

Zhou, H.-Y. et al., 2003, ApJ, 584, 147

MJD	R-mag (err)	P (err)	EVPA (err)	MJD	R-mag (err)	P (err)	EVPA (err)
5599.8	19.18 (0.02)	0.86 (0.50)	-32.08 (11.3)	6008.7	19.48 (0.02)	1.92 (0.39)	-46.7 (0.3)
5602.8	19.18 (0.02)	2.02 (0.30)	-36.9 (19.2)	6039.8	19.07 (0.02)	3.89 (0.61)	28.9 (13.5)
5705.7	18.21 (0.02)	1.35 (1.29)	93.4 (8.6)	6040.7	18.89 (0.03)	3.13 (0.36)	9.0 (1.7)
5706.7	17.88 (0.03)	12.31 (1.21)	22.6 (9.3)	6059.7	19.19 (0.03)	0.90 (0.28)	6.2 (62.7)
5708.7	18.90 (0.02)	4.00 (1.51)	11.7 (42.0)	6251.9	18.94 (0.02)	2.29 (0.69)	-44.0 (0.1)
5951.8	19.05 (0.03)	1.66 (0.26)	-50.74 (2.6)	6253.0	18.68 (0.02)	2.82 (0.58)	15.2 (3.6)
5982.8	18.678 (0.03)	1.70 (0.48)	19.4 (13.6)	6300.0	18.06 (0.03)	1.89 (1.26)	9.0 (6.5)
5983.8	18.82 (0.03)	5.95 (0.50)	-59.3 (2.0)	6301.0	18.86 (0.02)	2.62 (0.65)	-64.0 (3.0)
5984.7	18.61 (0.03)	2.45 (0.16)	19.9 (5.3)	6302.0	19.00 (0.04)	1.17 (0.28)	79.7 (27.2)
6007.8	18.71 (0.03)	8.17 (0.74)	58.4 (13.5)	6393.8	18.78 (0.02)	1.20 (0.11)	66.14 (1.4)

Table 1: Photopolarimetric observations of J0948+0022 obtained between February, 2011 and May, 2012. Columns are: (1) time of the observation in MJD (JD - 2.45e6), (2) optical R-band magnitude and (error), (3) percent polarization of target and (error), and (4) EVPA and (error).

JD	R-mag	R err	# images
2455599.79411	19.180	0.020	1
2455602.79159	19.179	0.024	1
2455624.71679	19.382	0.003	7
2455625.62464	19.129	0.003	16
2455626.34594	19.198	0.005	16
2455627.31249	19.004	0.003	28
2455627.80059	18.812	0.004	11
2455647.70671	18.761	0.002	18
2455648.34777	18.761	0.001	68
2455649.27107	18.798	0.001	84

Table 2: A sample of our optical data, binned at 1-day intervals as described in the text. Columns are: (1) time of the observations in JD, (2) optical R-band magnitude, (3) uncertainty in the magnitude, and (4) the number of observations used to create the binned data point. The full table of 114 values used in this work can be found in the online version of this manuscript.

MJD	R-mag (err)	$\Delta R$ (err)	$\Delta J$ (err)
6360.5	17.271 (0.016)	-1.373 (0.026)	-1.375 (0.028)
6363.5	18.644 (0.021)	1.504 (0.030)	1.334 (0.028)
6364.5	17.140 (0.021)	-0.880 (0.028)	-0.793 (0.028)
6368.5	18.020 (0.018)	N/A	N/A

Table 3: Data corresponding to the strong optical flaring we observed in March, 2013. Columns are: (1) time of the observations in MJD, (2) optical R-band magnitude, (3) difference in magnitude between the measurement of the current row and next row, and (4) same as (3), but for the J-band data.

R-band Data			6-hr $\gamma$ -ray Bins			
MJD	$M_R(\text{err})$	$\tau_R$	MJD	Flux (err)	TS	$\tau_\gamma$
5652.61	18.69 (0.02)	4.39 (0.19)	6292.15	2.78 (1.67)	14.05	2.81 (4.23)
5652.79	17.92 (0.02)		6292.40	12.21 (5.61)	15.66	
6298.88	18.13 (0.04)	3.60 (0.23)	6292.65	8.26 (7.49)	12.03	4.28 (7.47)
6299.04	18.96 (0.02)		6292.90	21.81 (8.723)	14.91	
Average $\tau_R$		3.99 (0.15)	Average $\tau_\gamma$			3.55 (4.29)

Table 4: Data used to calculate doubling/halving timescales for optical and  $\gamma$ -ray data. Columns are (1) time (MJD) of the optical observation, (2) magnitude (error) in the R-band, (3) timescale  $\tau_R$  (in hours) calculated on from the two adjacent data points in Column 2, (4) mid-point in time of the 6-hour bin from which (5) the photon flux (error) in  $\text{ph}^*\text{cm}^{-2}*\text{s}^{-1}$  was derived, (6) the TS value of the aforementioned  $\gamma$ -ray data, and (7) the timescale  $\tau_\gamma$  calculated from the adjacent  $\gamma$ -ray data. The bottom row gives the average values and (uncertainties) for  $\tau$  in each waveband.

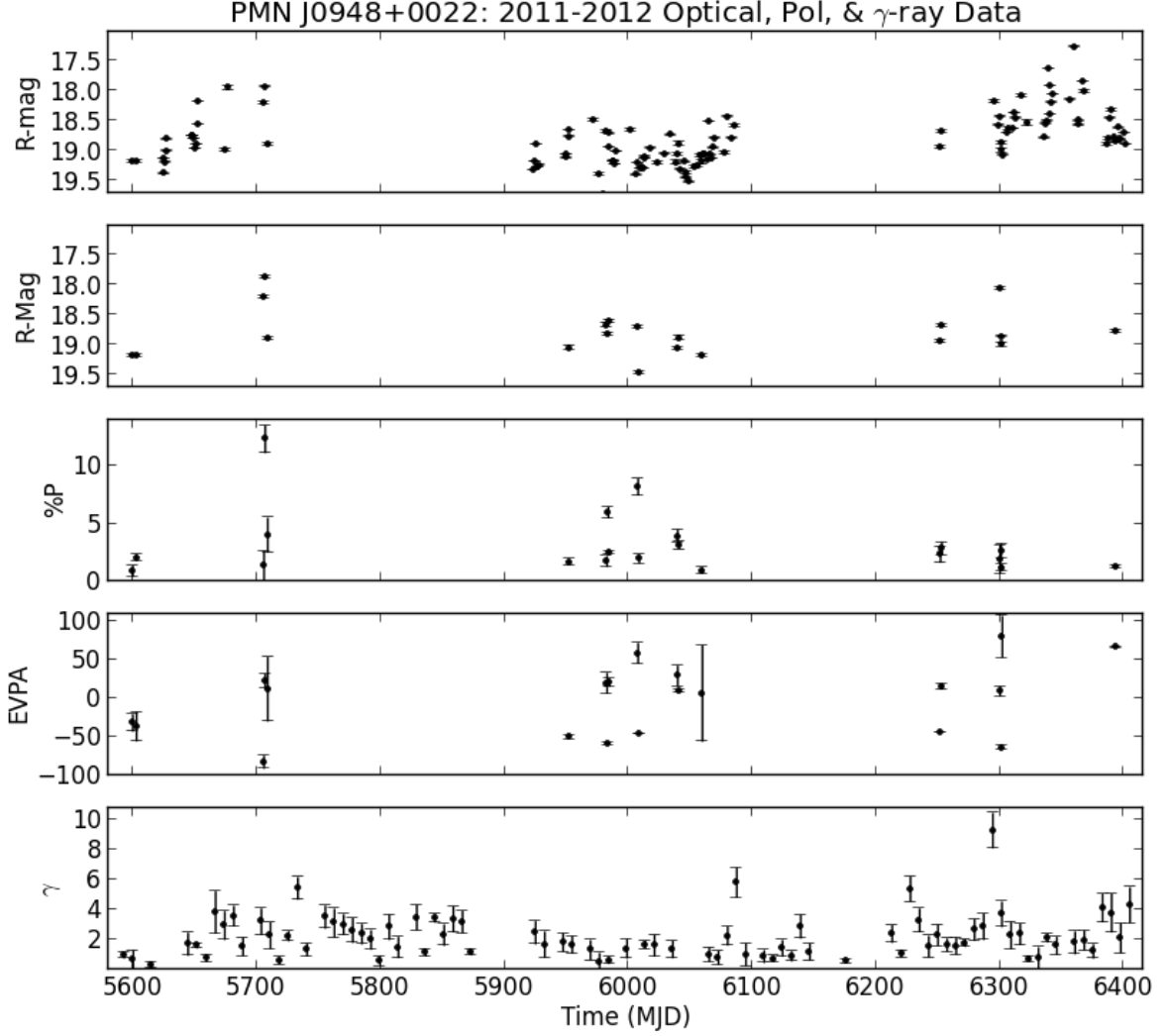


Fig. 1.— A comparison of all R-band optical data binned at 24-hour intervals (top panel), only optical data obtained with polarimetry (second panel), the Percent Polarization (third panel), position of the electric vector in degrees (fourth panel), and the integrated  $\gamma$ -ray flux (bottom panel) of PMN J0948+0022. Upper limits have been removed for clarity. Details on the photopolarimetric data can be found in Table 1. The same horizontal axis is common to all five plots.

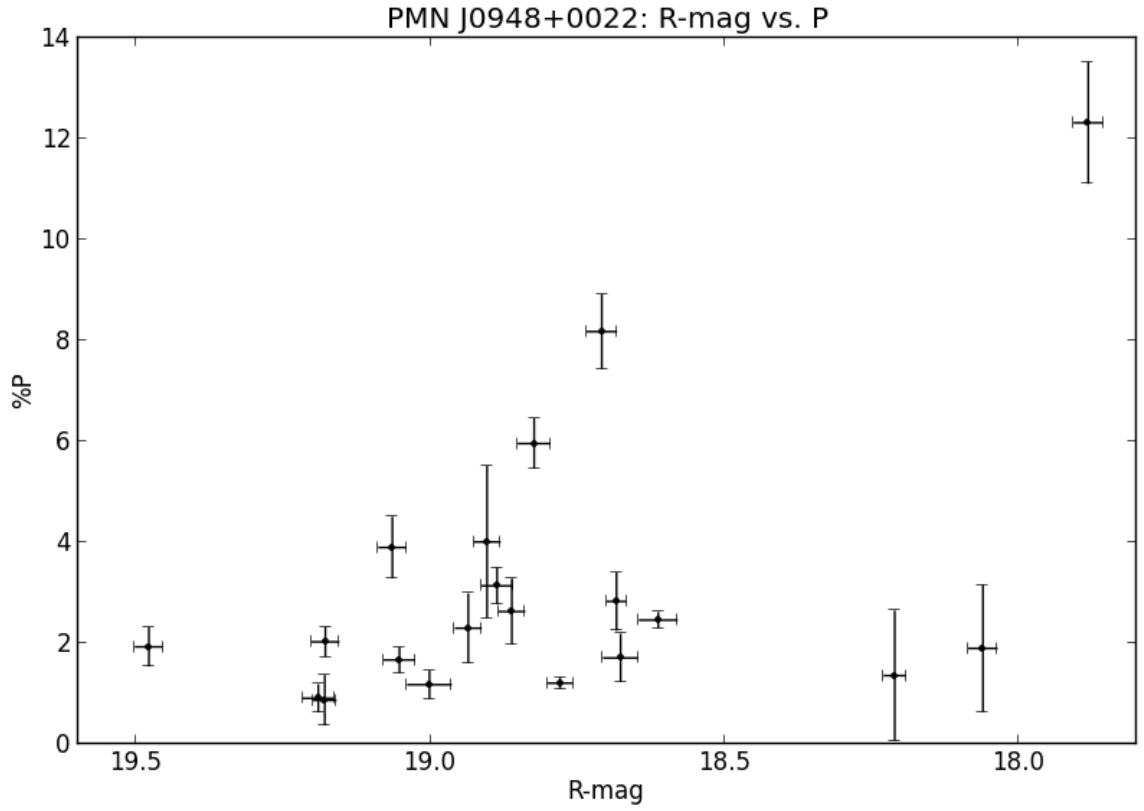


Fig. 2.— A plot of concurrent R-band magnitudes and P, based on the data in Table 1 so that each data point represents a measurement of the value of P and the R-magnitude that coincide in time.



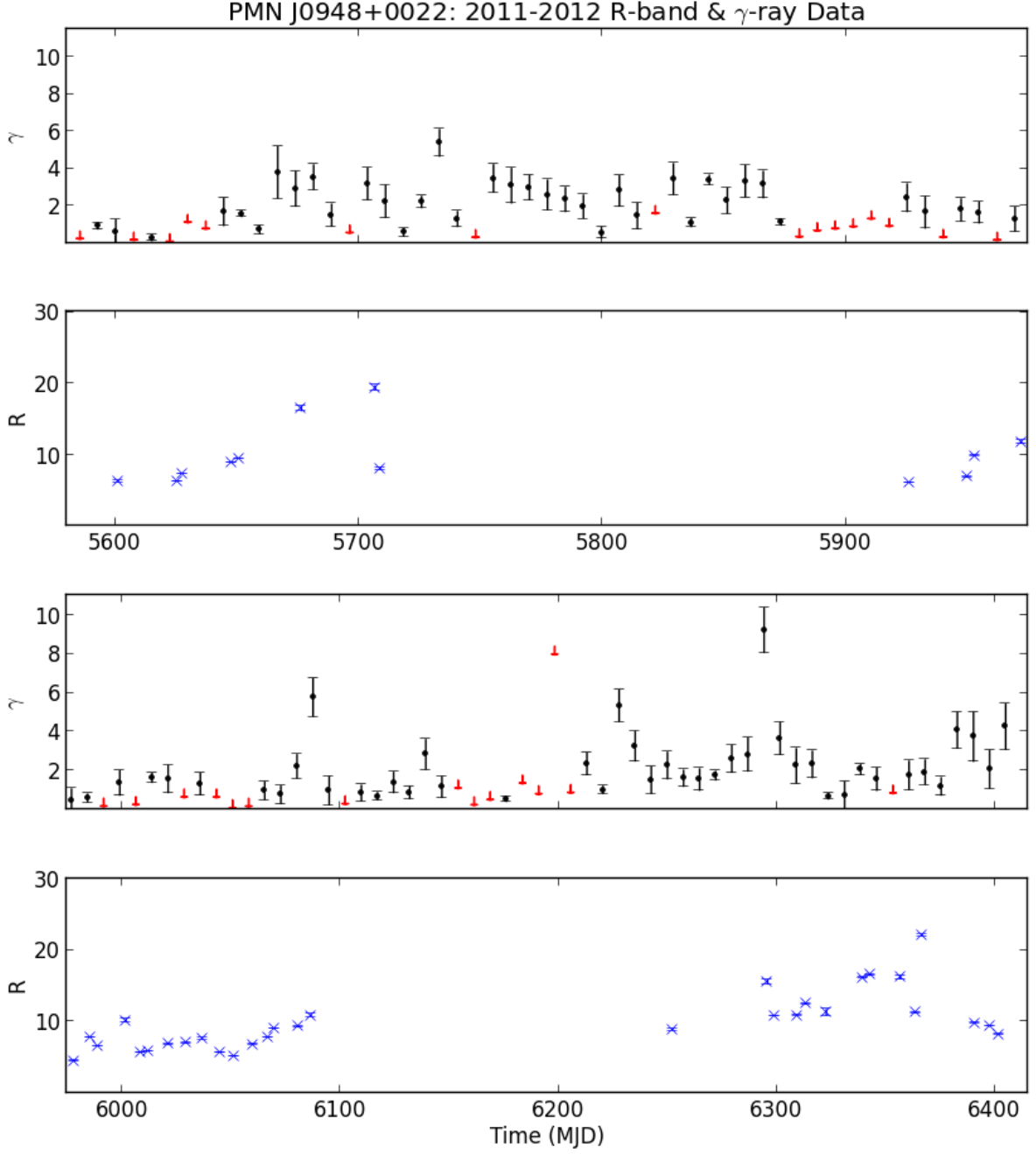


Fig. 3.—  $\gamma$ -ray flux (integrated from 100 MeV to 300 GeV) plotted in panels 1 & 3, with time-averaged R-band flux plotted in panels 2 & 4. Panels 1 & 2 share a common horizontal (time) axis, as do panels 3 & 4. Downward-pointing arrows denote upper-limits on  $\gamma$ -ray data points.

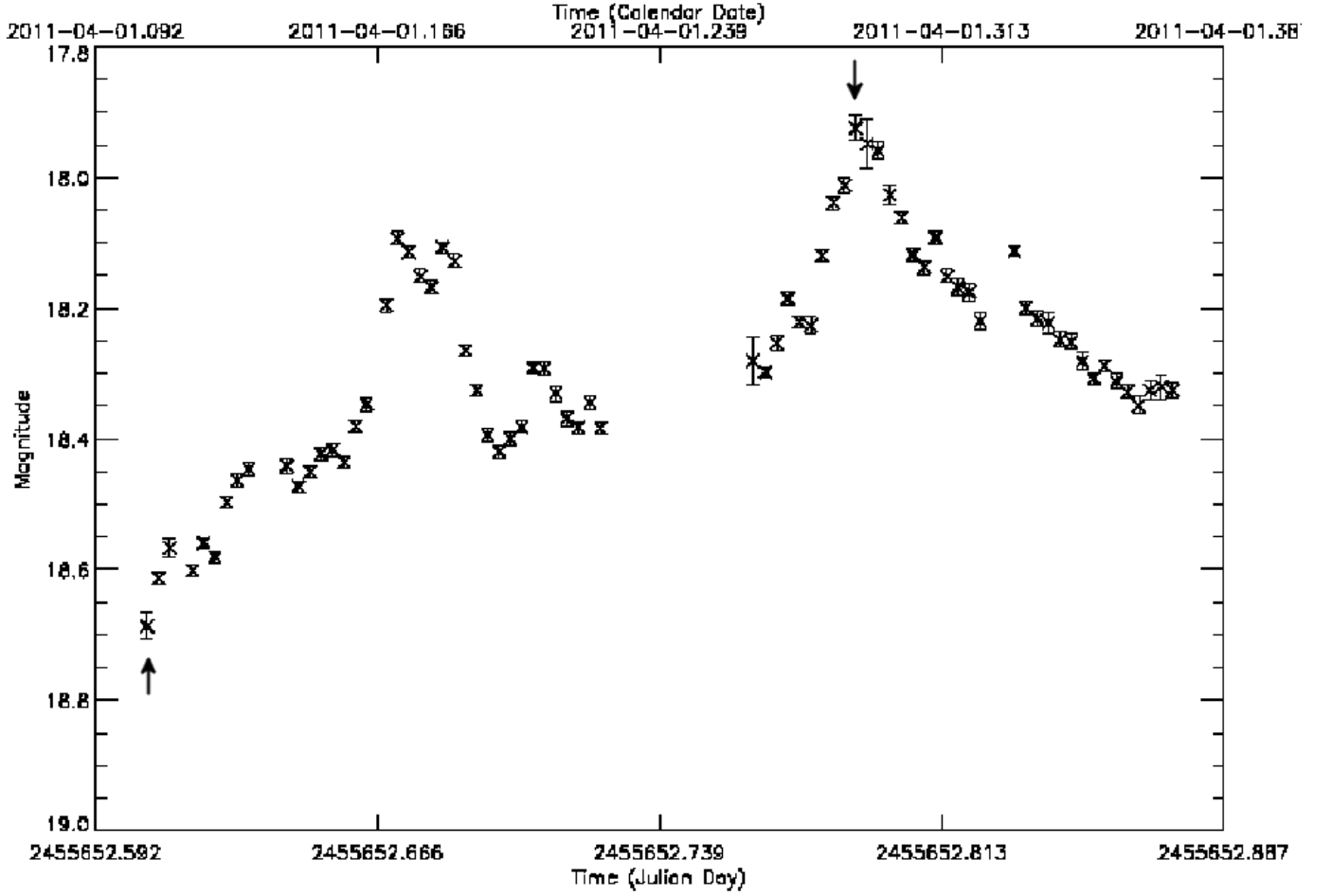


Fig. 4.— Microvariability data presented in Maune et al. (2013), showing the doubling of the flux in  $4.39 \pm .19$  hours. Arrows indicate the data points separated by the necessary flux difference and used to make the timescale calculation. Two discrete, roughly symmetric flares can also be seen in this figure.

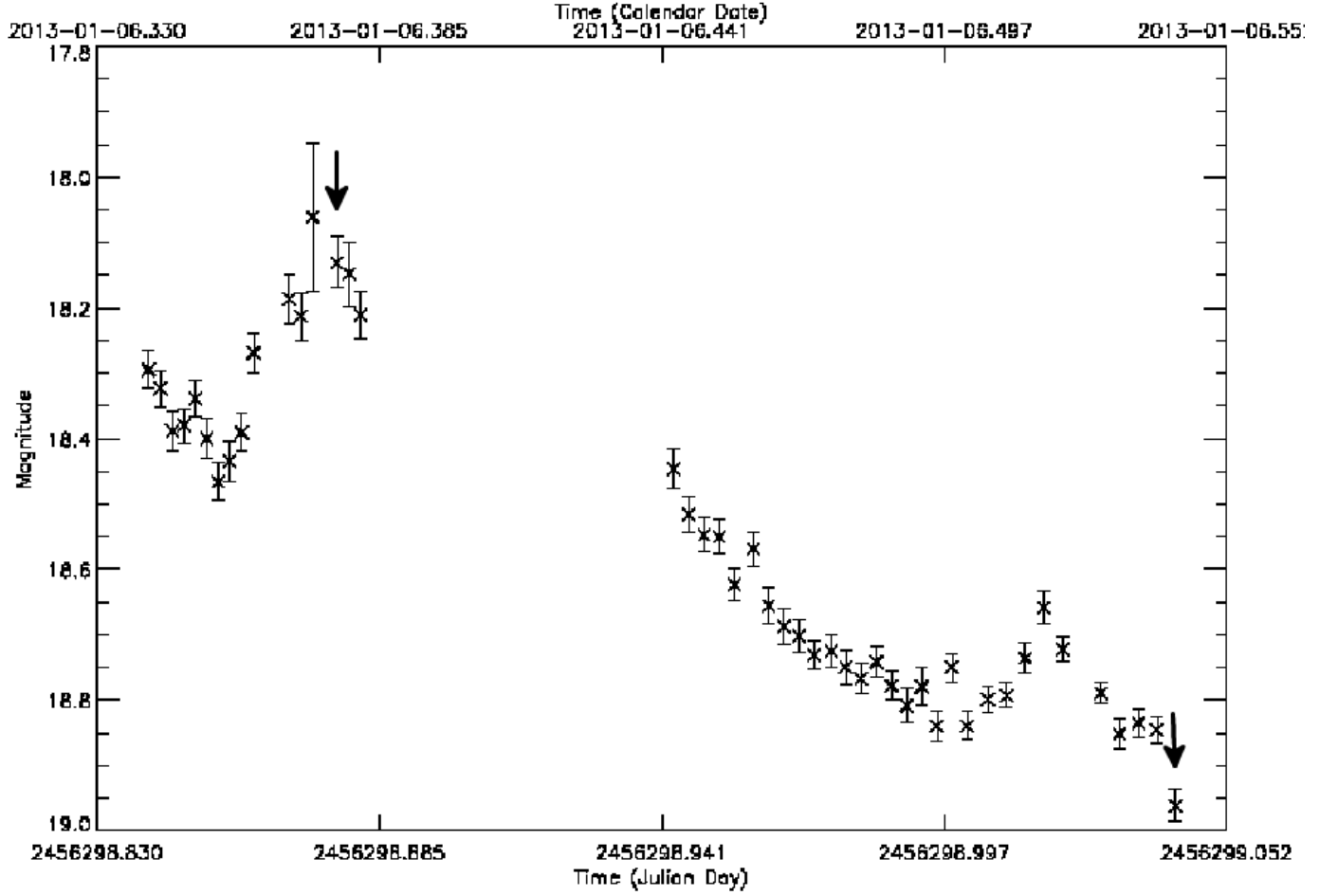


Fig. 5.— Similar to Figure 4, but original to this work and showing a halving of the total optical flux in  $3.60 \pm .23$  hours. Note the discrete flare near the end of the lightcurve.

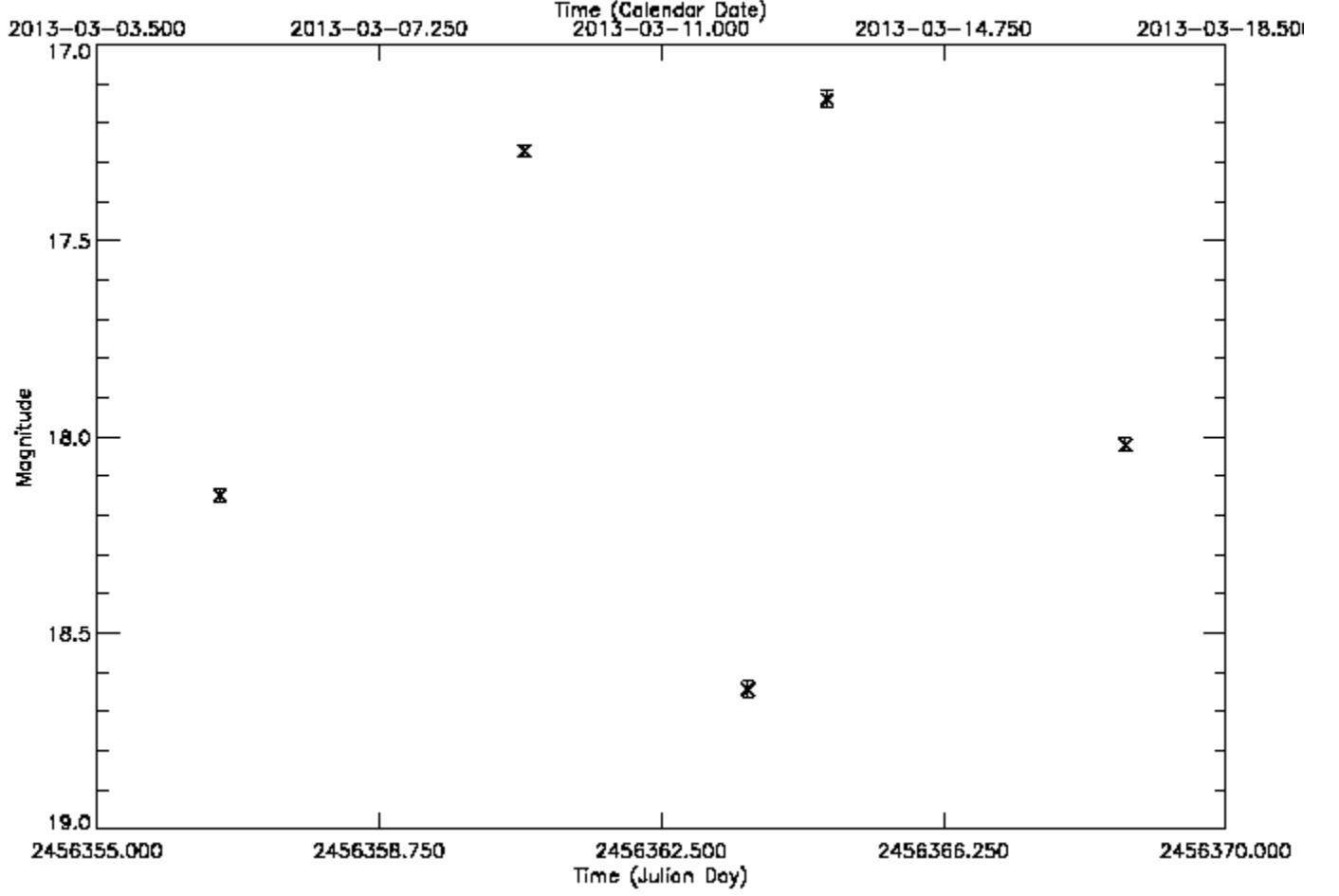


Fig. 6.— R-band optical data showing a rapid and dramatic rise in the flux of PMN J0948+0022 which appeared to be uncorrelated with any  $\gamma$ -ray activity. See Table 3 for the specifics of the observations.

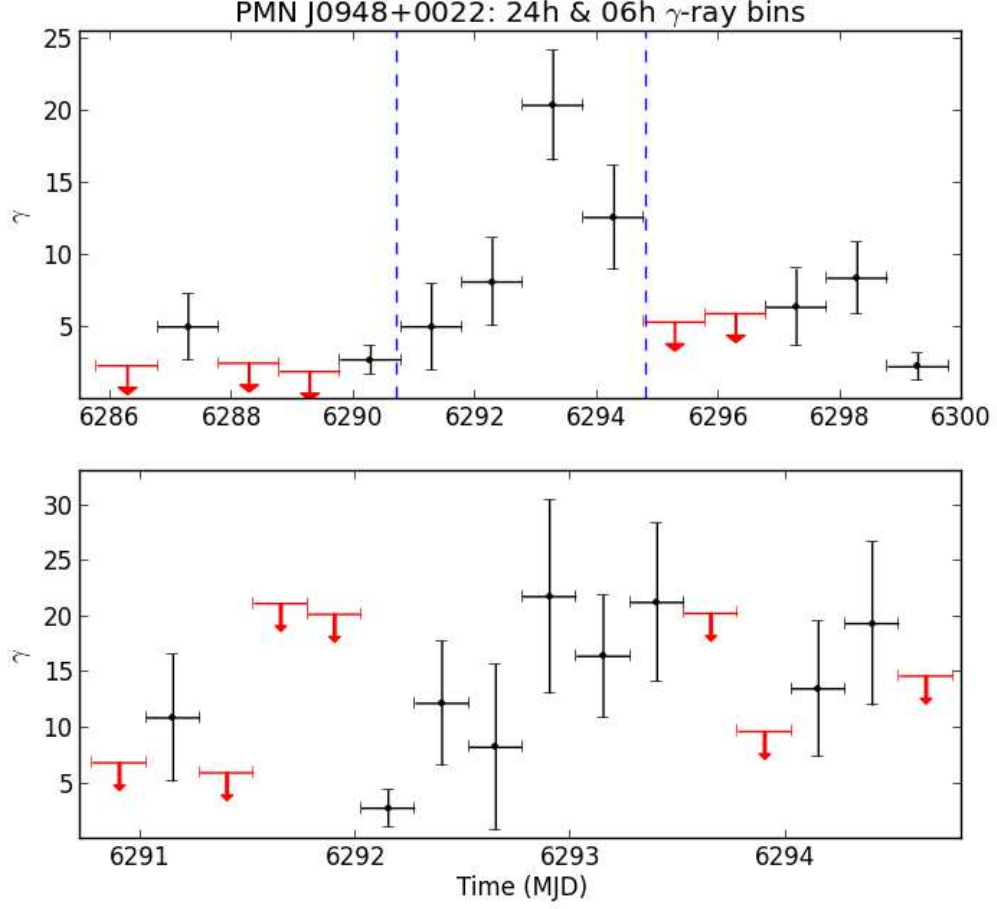


Fig. 7.— Top:  $\gamma$ -ray light curve centered on the high flux measurement which occurred on MJD = 6294 in Figure 3 with 24-hour time bins. Bottom: The data circumscribed by the blue dashed lines in the top panel, but analyzed with 6-hour time bins.

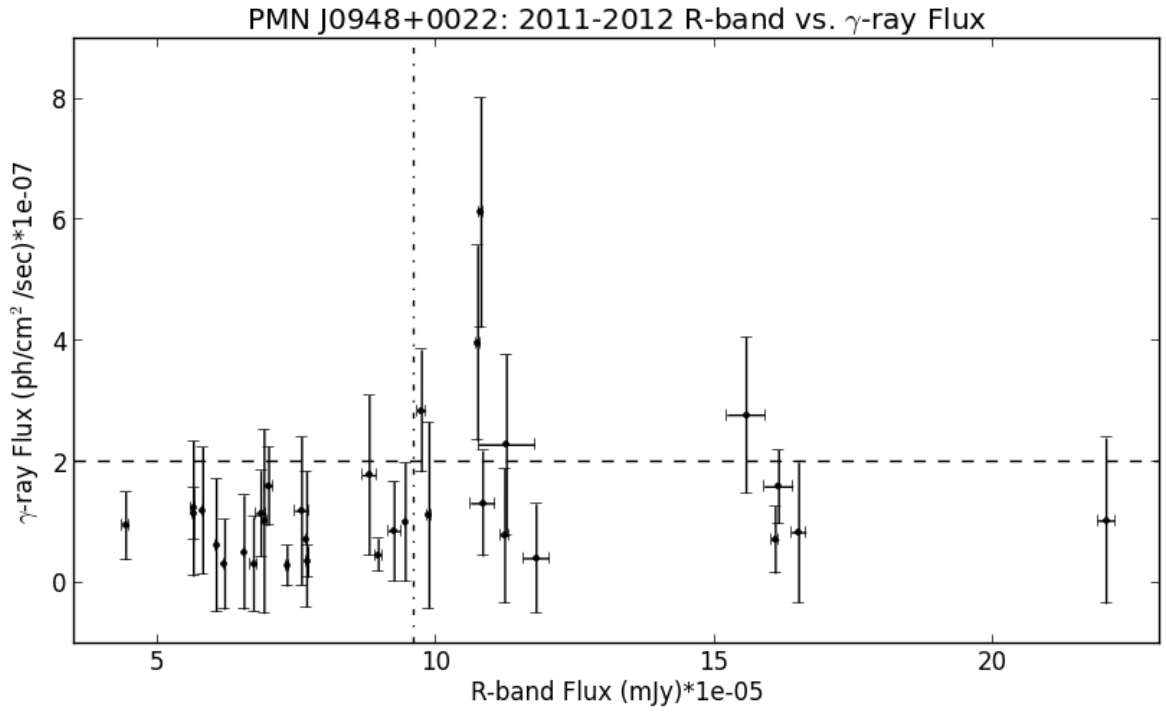


Fig. 8.— A plot of concurrent R-band and linearly-interpolated gamma-ray fluxes.